

Digital Pseudoquantum Simulation of \mathbb{Z}_2 Gauge Higgs Model

Yiming Ding^a Xiaopeng Cui^a Yu Shi^{a,1}

^a*Department of Physics & State Key Laboratory of Surface Physics, Fudan University, Shanghai 200433, China*

E-mail: 19210190001@fudan.edu.cn, 16110190045@fudan.edu.cn,
yushi@fudan.edu.cn

ABSTRACT: We perform a digital pseudoquantum simulation of \mathbb{Z}_2 gauge Higgs model on a 3×3 lattice. First we propose the quantum algorithm for the digital quantum simulation, based on Trotter decomposition, quantum adiabatic algorithm and its circuit realization. Then we classically demonstrate it in a GPU simulator, obtaining useful results, which indicate the topological properties of deconfined phase and clarify the phase diagram. Especially, our work suggests that the tricritical point, where the two critical lines of second-order transitions meet, lies on the critical line of the first-order transition rather than its end.

¹Corresponding author.

Contents

1	Introduction	1
2	Model description	3
3	Digital quantum simulation based on quantum adiabatic algorithm	3
4	Preparation of initial state	5
5	Phase diagram	8
6	Error analysis	12
7	Summary	13
A	Calculation of the Trotter errors	13

1 Introduction

Lattice gauge theory is a nonperturbative approach to gauge theory, and is important in particle physics, condensed matter physics and even topological quantum computing [1]. It is usually implemented in terms of Monte Carlo simulation, which, however, lacks real-time dynamics and may suffer the well known sign problem of fermions.

Recently, quantum simulation has appeared to be able to dissolve these problems [2–5]. As done for pure \mathbb{Z}_2 gauge theory [5, 6], for a quantum simulation involving only dozens of qubits, it is very useful to make classical demonstration in a high-performance platform, which we call pseudoquantum simulation. It not only serves as benchmark for real quantum simulation and facilitates the development of quantum algorithms, but is also a new numerical method for computational problems.

An extension of the \mathbb{Z}_2 pure gauge theory is the \mathbb{Z}_2 gauge Higgs model, which contains coupling between matter and gauge fields. There exists duality between the gauge field and the matter field in this model, which is equivalent to the transverse-field toric code model [7]. This model has been widely studied analytically [8–11] and numerically [7, 12–14]. It has been known that in this model (cf. Fig. 1), there is a deconfined phase, separated from a confined phase on one hand, and from a so-called Higgs phase on the other. The phase transition between the deconfined and the confined or Higgs phase is second-order, leading to a topological region surrounded by two second-order lines on the phase diagram. These two lines meet at a self-dual point. The confined and Higgs phases are separated by a finite dual line of a first-order transition, beyond which the two phases are continuously connected.

However, with strong competition between matter and gauge fields, how these critical lines are connected and where the two second-order lines meet were not yet clear previously. It was pointed out that there are three possibilities [7]. A quantum Monte Carlo (QMC) study provides the evidence that the tricritical point, where the three critical lines meet, is scale-invariant and second-order [14].

In this paper, we report a digital pseudoquantum simulation of \mathbb{Z}_2 gauge Higgs model. It is digital as it is based on Trotter decomposition of the unitary evolution. It realizes the quantum adiabatic algorithm in terms of quantum circuits. Our pseudoquantum simulation is its classical demonstration by using a GPU simulator called Quantum Exact Simulation Toolkit (QuEST) in a NVIDIA GeForce RTX 3090 GPU server.

We have investigated the quantum phase transition, the dynamic process along the dual line on the phase diagram, and the behavior near the tricritical point. Especially, our work suggests that the tricritical point, where the two second-order lines end, lies on the line of the first-order transition, rather than at the lower end of it (see Fig. 1).

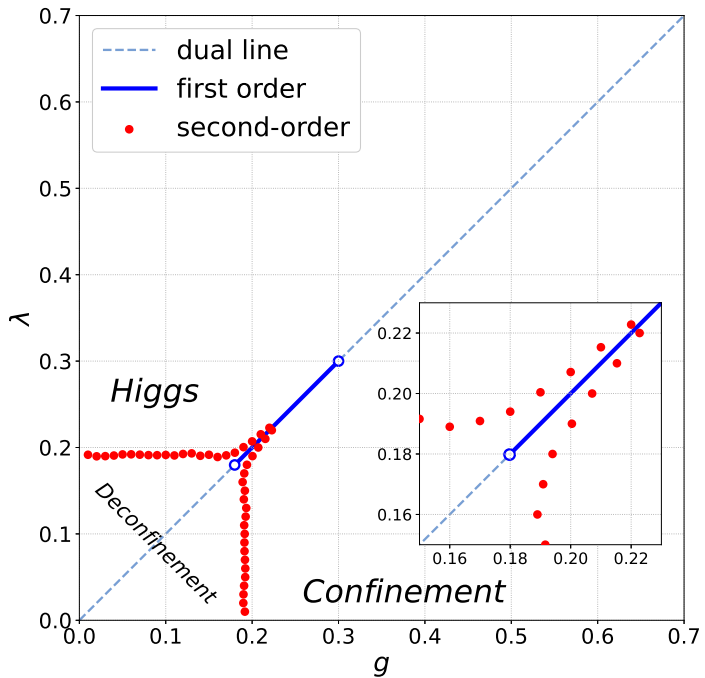


Figure 1. The phase diagram from our calculation. The red points represent the second-order transitions and the blue line represents first-order transitions. The first-order transition line has not only a part outside the deconfined phase, but also a small part within the deconfined phase.

The rest of the paper is arranged as the following. In Sec. 2, we briefly introduce the \mathbb{Z}_2 gauge Higgs model. In Sec. 3, we elaborate the digital quantum adiabatic algorithm and its realization in terms of quantum circuits. In Sec. 4, we describe the preparation of initial state, as well as the topological phase. In Sec. 5, we analyze the critical points according to the analysis of the density of states (DOS). The Trotter error is analyzed in

Sec. 6, with some details in the Appendix. A summary is made in Sec. 7.

2 Model description

The Hamiltonian of the \mathbb{Z}_2 gauge-Higgs model is

$$H = -J \sum_v \tau_v^x - h \sum_p B_p^z - g \sum_l \sigma_l^x - \lambda \sum_{\langle j,k \rangle} \tau_j^z \sigma_{\langle j,k \rangle}^z \tau_k^z, \quad (2.1)$$

where σ denotes gauge fields on links and τ denotes Ising matter fields at vertices,

$$B_p^z = \prod_{j \in \partial p} \sigma_j^z, \quad (2.2)$$

is the tensor product of four σ^z 's on the sides of a plaquette p . The Gauss' law is given by

$$Q_v^x = \tau_v^x \prod_{j \in \partial v} \sigma_j^x \equiv \tau_v^x A_v^x. \quad (2.3)$$

Under a mathematical mapping, Eq. (2.1) is equivalent to a toric code model with two transverse fields [7], which is used in our work. We focus on the parameter subspace with $J = h = 1/2$, that is,

$$H = -\frac{1}{2} \sum_v A_v^x - \frac{1}{2} \sum_p B_p^z - g \sum_l \sigma_l^x - \lambda \sum_l \sigma_l^z. \quad (2.4)$$

The total number of qubits is 19, one for ancilla and the others for a 3×3 lattice model on torus.

3 Digital quantum simulation based on quantum adiabatic algorithm

Our purpose is to obtain the energy of the system as a function of parameters λ and g . Since this model possesses an intrinsic duality, we only need to investigate the behavior below the dual line $\lambda = g$ on the parameter plane $\lambda - g$. The g axis in this model represents pure \mathbb{Z}_2 gauge theory, for which we prepare the initial ground state on a point $P(p, 0)$ on the g axis.

Then two kinds of paths of parameter variation are used for the adiabatic algorithm (See FIG. 2). On a red path, the parameters vary first to $R(p, r)$, then to $R'(0, r)$. On a blue path, the parameters vary from $P(p, 0)$ to $P'(0, p)$ on the straight line.

In this section, we introduce the algorithm for the digital quantum simulation, which is implemented by using quantum circuit, and use quantum adiabatic algorithm to evolve the ground state along paths in the parameter space. For convenience, we write

$$H = H_1 + H_2 + H_3, \quad (3.1)$$

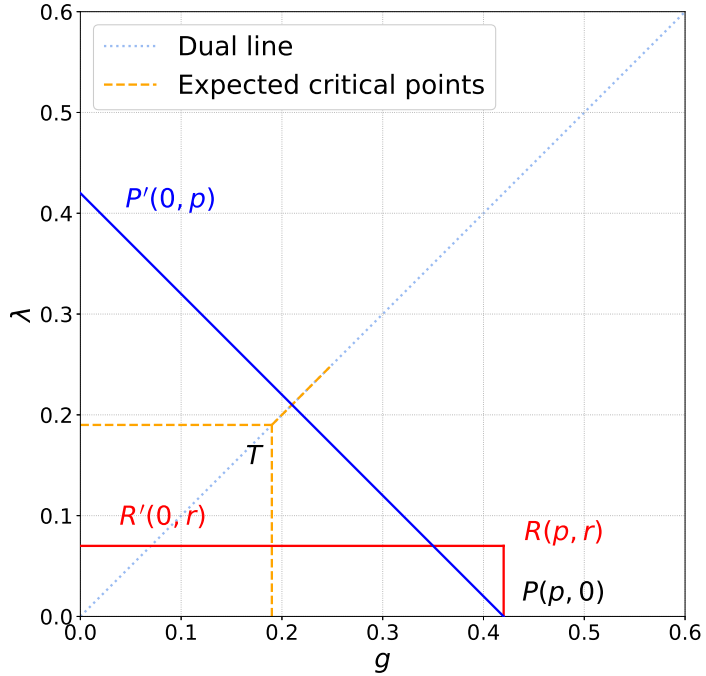


Figure 2. Two paths in our simulations.

where

$$\begin{aligned}
 H_1 &= -g \sum_l \sigma_l^x, \\
 H_2 &= -\frac{1}{2} \sum_v A_v^x - \frac{1}{2} \sum_p B_p^z, \\
 H_3 &= -\lambda \sum_l \sigma_l^z
 \end{aligned} \tag{3.2}$$

We decompose the evolution operator e^{-iHt} with second-order Trotter-Suzuki formula [15],

$$e^{-iHt} \approx e^{-iH_1 \frac{t}{2}} e^{-iH_2 \frac{t}{2}} e^{-iH_3 t} e^{-iH_2 \frac{t}{2}} e^{-iH_1 \frac{t}{2}}, \tag{3.3}$$

where

$$\begin{aligned}
 e^{-iH_1 \frac{t}{2}} &= \prod_l e^{ig\sigma_l^x \frac{t}{2}}, \\
 e^{-iH_2 \frac{t}{2}} &= \prod_v e^{i\frac{1}{2}A_v^x \frac{t}{2}} \prod_p e^{i\frac{1}{2}B_p^z \frac{t}{2}}, \\
 e^{-iH_3 t} &= \prod_l e^{i\lambda\sigma_l^z t}.
 \end{aligned} \tag{3.4}$$

This decomposition does not generate errors, since the summands in H_j commute with each other.

$e^{-iH_1\frac{t}{2}}$ and e^{-iH_3t} can be realized by using two sets of rotation gates R_x 's and R_z 's

$$\begin{aligned} \prod_l e^{ig\sigma_l^x \frac{t}{2}} &= \prod_l R_x^l(-gt), \\ \prod_l e^{i\lambda\sigma_l^z t} &= \prod_l R_z^l(-2\lambda t). \end{aligned} \quad (3.5)$$

By introducing an ancilla a , each $e^{i\frac{1}{2}B_p^z \frac{t}{2}}$ can be realized as

$$e^{i\frac{1}{2}B_p^z \frac{t}{2}} = U_1 [R_z(-\frac{t}{2})]_a U_1^\dagger, \quad (3.6)$$

where

$$U_1 = \prod_{j \in p} \text{CNOT}_{j \rightarrow a}. \quad (3.7)$$

$e^{i\frac{1}{2}A_v^x \frac{t}{2}}$ can be realized similarly, and we only need 4 additional Hadamard gates to switch into z basis the 4 spins on the sides connected at v , that is

$$e^{i\frac{1}{2}A_v^x \frac{t}{2}} = U_2^\dagger [R_z(-\frac{t}{2})] U_2, \quad (3.8)$$

where

$$U_2 = \left[\prod_{k \in v} \text{CNOT}_{k \rightarrow a} \right] \left[\prod_{k \in v} H_k \right]. \quad (3.9)$$

Note that we use the convention for the time order of operators, that is, from right to left. We omit drawing the circuits, which is straightforward.

To ensure the adiabaticity in the variation of the parameters, evolution on each path is divided into numerous tiny steps, each with the same time duration.

4 Preparation of initial state

The initial ground state at $P(p, 0)$ is the same as an intermediate state in our previous work on the pure \mathbb{Z}_2 gauge theory [5], as the mere addition of A_v does not affect the state.

To prepare the ground state from $|00 \dots 00\rangle$, we use the circuit of

$$\prod_p \left\{ \left[\prod_{j \in p} \text{CNOT}_{j \rightarrow a} \right] [\text{P}_{a=|0\rangle}] \left[\prod_{j \in p} \text{CNOT}_{j \rightarrow a} \right] \right\} \prod_l H_l. \quad (4.1)$$

The idea is to first generate the equal superposition of all the computational basis states, by using a set of hadamard gates on all the qubits, then for each plaquette, to apply four CNOT gates to transfer the relevant information on each basis state onto an ancilla. P represents the projection of the ancilla to be $|0\rangle$, which is feasible in the pseudoquantum computing. It leads to a superposition of all possible configurations with $B_p = 1$ for every p ,

which is also the ground state of a toric code at $O(0, 0)$ on $\lambda - g$ plane. The state prepared by using (4.1) is denoted as ψ_1 .

Then we adiabatically evolve ψ_1 along g axis, by using the circuit-based digital quantum adiabatic algorithm in Sec. 3. Finally we reach the ground state at $P(p, 0)$.

Note that if we initially prepare a ground state at $P'(0, p')$, ψ_1 should be replaced correspondingly according to the duality.

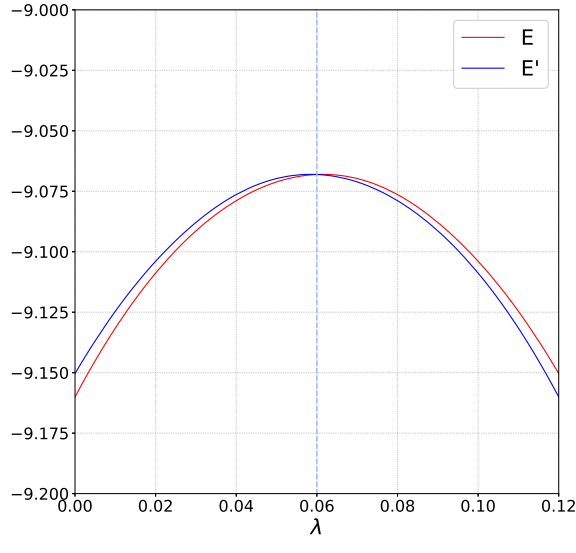
As the ground state of \mathbb{Z}_2 gauge theory can be described by 't Hooft loop operator V_μ^x and non-contractible Wilson loop operator W_ν^z , the eigenstates of V_μ^x on g axis are dual to the eigenstates of W_ν^z on the λ axis. To obtain the ground state at P' , the state prepared at $O(0, 0)$ is $\psi'_1 = (\psi_1 + \psi_2 + \psi_3 + \psi_4)/2$, where ψ_2, ψ_3 and ψ_4 are degenerate with ψ_1 at O .

Similarly, the quantum circuit for ψ'_1 is

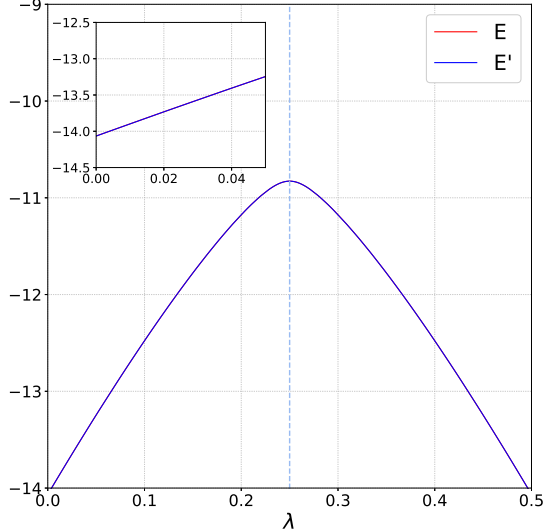
$$\prod_v \{ [H_k \prod_{k \in v} \text{CNOT}_{k \rightarrow a}] [\text{P}_{a=|0\rangle}] [\prod_{k \in v} \text{CNOT}_{k \rightarrow a} H_k] \}. \quad (4.2)$$

ψ_1 and ψ'_1 are also degenerate at O . If the evolution is restricted in a topological phase, they cannot evolve to each other because of the topological protection. In other words, the evolution from $P(0, p)$ to $P'(0, p')$ should be different from that on the reversed path.

We prepare each of these two ground states on the corresponding parameter point and evolve it to the other parameter point along the blue path in Fig. 2. The result shows that these two energy curves cross if the path is chosen within the deconfined phase, and do not cross if the path is outside of the deconfined phase, as indicated in Fig. 3.



(a)



(b)

Figure 3. Energy as a function of λ along the blue path. (a) For $p = p' = 0.12$, $E' = -9.16003$ and $E = -9.15039$, where E' is the energy for the state evolved from that prepared at P , while E is the energy for the state prepared at P' . Two energy curves cross, indicating a topological phase. (b) For $p = p' = 0.50$, $E' = -14.06550$ and $E = -14.06553$. Two energy curves nearly coincide and the energy is symmetric with respect to the center of the blue path, indicating a nontopological phase.

5 Phase diagram

We now determine the critical points of quantum phase transitions as the extreme points in the second derivatives of the energy.

After numerous trials, we choose $p = 0.5$ for the red path in Fig. 2, of which the λ value denoted as r . The results show that for $r < 0.19$, the critical value of g is $g_c \approx 0.19$, while for $r > 0.19$, $g_c \approx r$, as depicted in Fig. 4. In this way, we find that the two critical lines surrounding the deconfined phase meet at $g \approx 0.24$, as shown in Fig. 1.

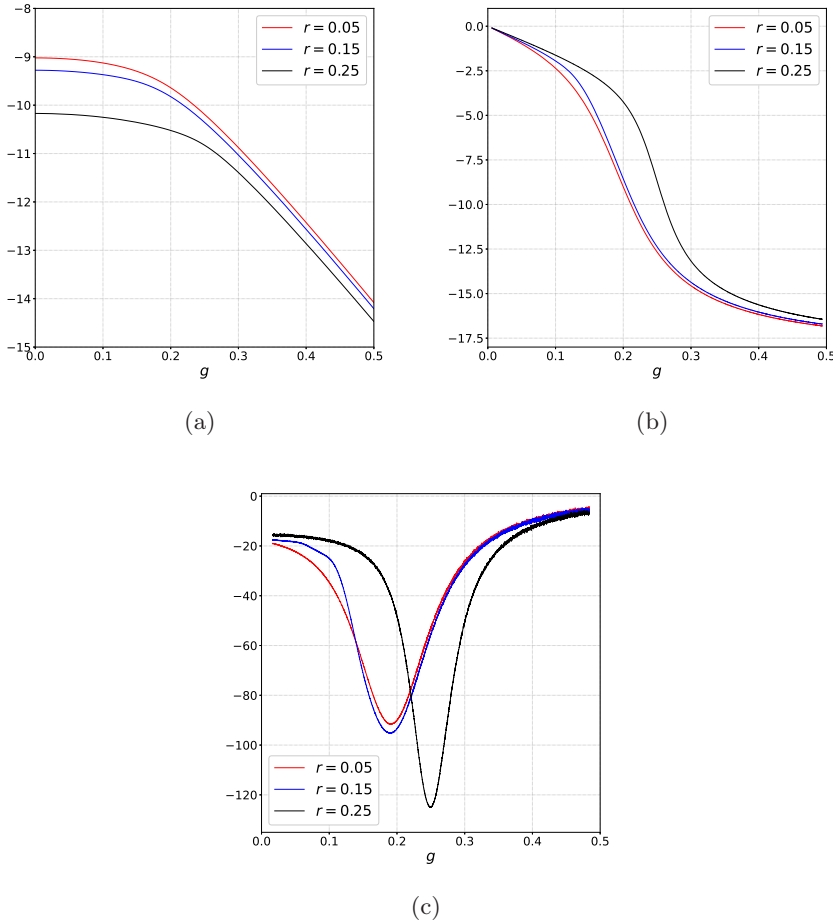


Figure 4. For the λ value $r = 0.05, 0.15, 0.25$ on red paths (see Fig. 2), (a) energy, (b) first derivative of the energy, (c) second derivative of the energy, as functions of g . The minima in (c) are at 0.1920, 0.1916 and 0.2489 respectively.

As shown in Fig. 5, we determine the order of the quantum phase transition according to the DOS (density of states) of the eigenstates of $\tilde{Z} = -\sum_l \sigma_l^z$, as in our previous work. When $r < 0.16$, the DOS of \tilde{Z} shows only one maximum before and after the critical point, respectively. This is same as in the pure \mathbb{Z}_2 gauge theory. Hence the quantum phase transition is of second-order. This verifies that the two critical lines surrounding the deconfined phase are second-order.

Such kind of DOS becomes more and more disordered when $r > 0.16$, which represent the region close to the meeting point T of the two second-order critical lines on the phase diagram. Similar phenomena can also be observed on blue paths.

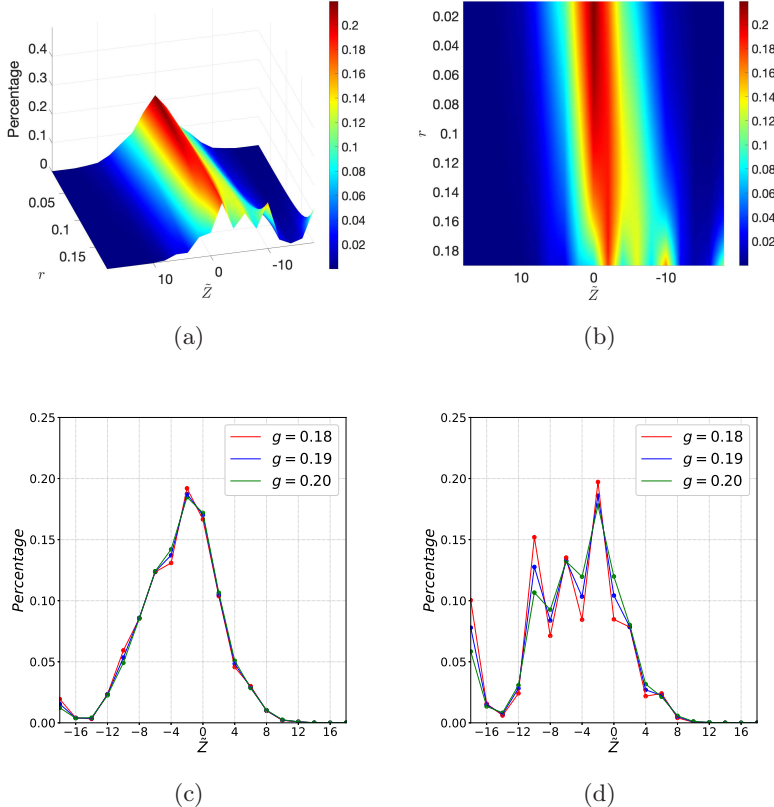


Figure 5. (a) (b) DOS of \tilde{Z} for $g = 0.19$ and $r \in [0.01, 0.19]$ on red paths. (c) DOS of \tilde{Z} for $r = 0.14$. (d) DOS of \tilde{Z} for $r = 0.18$.

A characteristic feature of the first-order phase transition is the coexistence of different phases. The conversion from single-maximum to multi-maxima of the DOS of \tilde{Z} is then regarded as the conversion from second-order phase transition to first-order phase transition.

As our system is small, although the multi-maxima feature appears in DOS when $r > 0.16$ in red paths, the first-order phase transition may not actually appear when $0.16 < g < 0.24$. It is likely that it appears only after the two second-order lines cross at $g \approx 0.24$.

Besides, no matter what value p we choose for the blue path, we can always observe an extreme point of d^2E/dg^2 right on the dual line, as shown in Fig. 7. Yet, an extreme point does not have to be a critical point. To determine the end of the first-order phase transition line outside the deconfined phase, we investigate the DOS of \tilde{Z} .

Since the Higgs phase and confined phase are continuously connected when $g, \lambda \rightarrow \infty$ [8], the first-order line should vanish somewhere. Fig. 6 shows the variation of the DOS on the dual line and gives two special points, $g_1 = 0.30$ and $g_2 = 0.65$. We consider g_1 as the end of the line because the maxima at $\tilde{Z} = -10$ indicates that the system starts

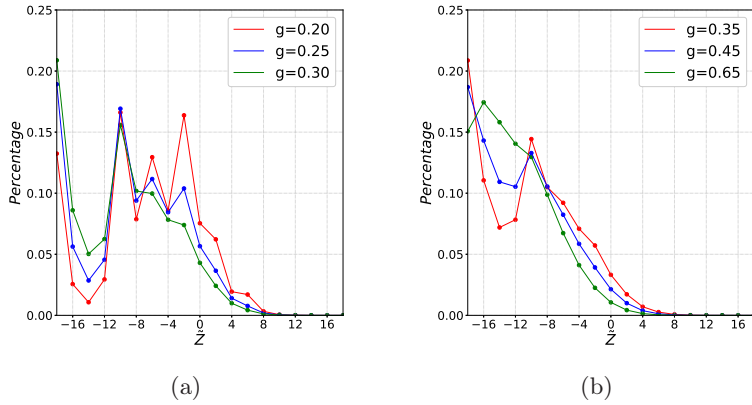


Figure 6. DOS of \tilde{Z} on the dual line. The disorder recedes as g increase. (a) At $g \approx 0.30$, the multi-maxima is reduced to two maxima. (b) At $g \approx 0.65$, we detect a single maximum.

to mainly permit the excitation of the smallest loop, which is composed of four spins, and other possible configurations are generally disfavored. In other word, the system turns into confinement.

Besides, we should observe three extreme points when $0.19 < p < 0.48$ with blue paths in principle according to Fig. 1. However, such kind of diagram can only be clearly observed when $p < 0.28$. For $p > 0.28$, we observe a single extreme point on the dual line. We regard this phenomenon as a limitation of the size of the lattice, which makes the extreme point on the dual line indistinguishable with the two on both sides.

The extreme points on the dual line make it natural for us to see the energy curve right on the dual line, so we choose a new path from $(0, 0.5)$, through $(0.5, 0.5)$, and to $O(0, 0)$. Surprisingly we find an extreme point at $g_3 = 0.1798$, which is in the deconfined phase (See Fig. 8). As the DOS is also disordered in the corner of deconfined phase, we suspect that the first-order line will extend for a while in deconfined phase and ends at g_3 (See Fig. 1).

The phase diagram we obtain is similar to the diagram in [11], which is derived by perturbation theory. The difference lies in the extension of the first-order line in deconfined phase. The region near the tricritical point has not been clear. Our result corresponds to one of the possibilities proposed in [7].

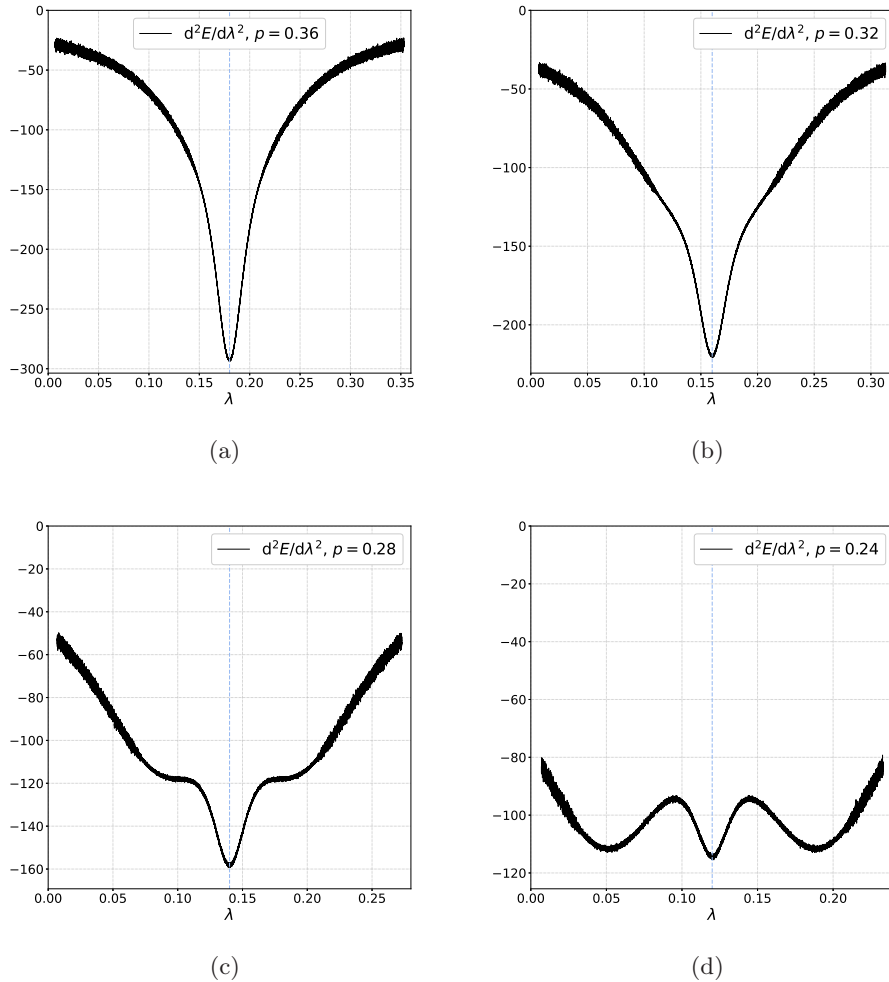


Figure 7. Energy as a function of λ , for blue paths with different values of p . (a) $p = 0.36$; (b) $p = 0.32$; (c) $p = 0.28$; (d) $p = 0.24$.

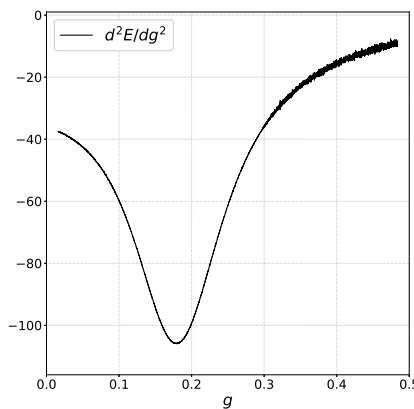


Figure 8. The second derivative of energy on the dual line, with an extreme point at $g = 0.1798 < 0.24$.

6 Error analysis

As the Trotter-Suzuki decomposition is used in each step, the upper bound of the total error should be a summation of the errors in each step.

We take the sub-path from $R(p, r) = (0.5, 0.05)$ to $R'(0, r) = (0, 0.05)$ as an example. As derived in Appendix, the accumulated Trotter error ϵ is

$$\epsilon \lesssim (\Delta t)^3 N (13.5p + 54pr^2 + 54pr + 54r^2 + 9p^2 + 18p^2r + 13.5r), \quad (6.1)$$

where Δt is the time for each step of varying the parameter values, N is the number of steps.

For variation of g from 0, Δg is the variation in each step. $\Delta g \propto \Delta t$. We choose $\Delta g = 10^{-5}$ and $\Delta t = 2 \times 10^{-2}$, giving $\epsilon \approx 4.581$, which seems to be too large for us. However, this error is achieved by adding the positive errors in all steps, the real errors are not always positive and may cancel with each other [16]. We demonstrate it in the following.

Rewrite $\Delta g = 0.0001/n$ and $\Delta t = 0.2/n$, then $n = n_0 = 10$ under the parameter values above. Define

$$\begin{aligned} \delta_n &= \sum_{g=0}^p |E_{n_0}(g) - E_n(g)| \\ \alpha_n &= \max_{g \in [0, p]} |E_{n_0}(g) - E_n(g)| \end{aligned} \quad (6.2)$$

where δ_n is a 1-norm of the difference between two energy functions $E_{n_0}(g)$ and $E_n(g)$, α_n represents the largest value of the difference. The results in TABLE 1 and Fig. 9 show that even ε at $n_0 = 10$ is around 6363 times more than that at $n = 800$, δ_n is merely 0.04075 and the maximal deviation α_n is only 0.005%. This is a direct evidence that the error at each step cannot always be positive, thus our choice of $n = 10$ is feasible.

n	Δg	Δt	ε	δ_n	α_n
10	1.00×10^{-5}	2.0×10^{-2}	4.58100	0	0
200	5.00×10^{-7}	1.0×10^{-3}	0.01145	0.03982	4.79×10^{-5}
500	2.00×10^{-7}	4.0×10^{-4}	0.00183	0.04009	4.99×10^{-5}
800	1.25×10^{-7}	2.5×10^{-4}	0.00072	0.04075	4.98×10^{-5}

Table 1. Different values of δ_n and α_n for $n = 10, 200, 500, 800$.

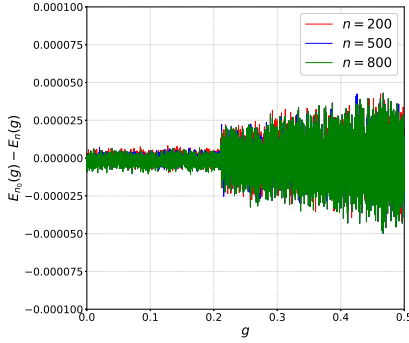


Figure 9. The diagram of difference $E_{n_0}(g) - E_n(g)$ for different values of n .

7 Summary

We have first designed the quantum simulation of \mathbb{Z}_2 gauge Higgs model. The quantum simulation is digital, as it is based on Trotter decomposition of the unitary evolution. It is also based on quantum adiabatic algorithm. For each parameter value, which is varied slowly, the Trotter decomposition is used to execute the unitary transformation. Within each step in the Trotter decomposition, the unitary transformations are realized in terms of simple quantum circuits.

Then we make a thorough classical demonstration of this quantum simulation by using QuEST simulator in a NVIDIA GeForce RTX 3090 GPU server. We call such an approach pseudoquantum simulation. We have performed a pseudoquantum simulation of \mathbb{Z}_2 gauge Higgs model on a 3×3 lattice. The lattice is small, as limited by computational time.

We have obtained some clear results on the topological properties of deconfined phase. Especially, our work suggests that the two lines of second-order transitions meet on the line of the first-order transition rather than its end.

A Calculation of the Trotter errors

It is useful to calculate $\|H_j\|$ and $\|[H_k, H_l]\|$ in advance where $\|\cdot\|$ denotes the spectral norm of an operator, or the largest singular value of it. We use the estimation that $\|O\| \sim 1$, where O is a Pauli operator or a tensor product of Pauli operators.

For our specific 3×3 lattice model (See Fig. 10), we have

$$\begin{aligned} \|H_1\| &\sim 18g, \quad \|H_3\| \sim 18\lambda \\ \|H_2\| &\leq \frac{1}{2} \left\| \sum_p B_p^z \right\| + \frac{1}{2} \left\| \sum_v A_v^x \right\| \sim 9 \end{aligned} \tag{A.1}$$

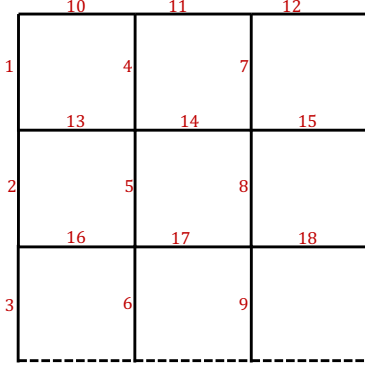


Figure 10. Lattice used in the simulations.

and

$$\begin{aligned}
& \| [H_1, H_2] \| \\
&= \| [-g \sum_l \sigma_l^x, -\frac{1}{2} \sum_p B_p^z - \frac{1}{2} \sum_v A_v^x] \| \\
&= \frac{g}{2} \| [\sum_l \sigma_l^x, \sum_p B_p^z] \| \\
&\leq \frac{g}{2} \sum_l \| [\sigma_l^x, \sum_p B_p^z] \| \\
&= 18 \frac{g}{2} \| [\sigma_4^x, \sum_p B_p^z] \| \\
&= 18 \frac{g}{2} \| [\sigma_4^x, \sigma_1^z \sigma_{10}^z \sigma_4^z \sigma_{13}^z] + [\sigma_4^x, \sigma_4^z \sigma_{11}^z \sigma_7^z \sigma_{14}^z] \| \\
&\sim 18g
\end{aligned} \tag{A.2}$$

where the coefficient 18 comes up due to the symmetry of the lattice. Similarly, we have $\| [H_2, H_3] \| \sim 18\lambda$ and

$$\begin{aligned}
& \| [H_1, H_3] \| \\
&= \| [-g \sum_l \sigma_l^x, -\lambda \sum_s \sigma_s^z] \| \\
&= g\lambda \| [\sum_l \sigma_l^x, \sum_s \sigma_s^z] \| \\
&= g\lambda \| \sum_l [\sigma_l^x, \sigma_l^z] \| \\
&\sim 36g\lambda
\end{aligned} \tag{A.3}$$

Multiplying a minus sign does not change the eigenvalues of a matrix, thus $\| [H_2, H_1] \| \sim 18g$, $\| [H_3, H_1] \| \sim 36g\lambda$ and $\| [H_3, H_2] \| \sim 18\lambda$.

Suppose $H = \sum_{\gamma=1}^{\Gamma} H_{\gamma}$, then the tight error bound for the second-order decomposition is [17]

$$\begin{aligned} \|S_2(\Delta t) - e^{-i(\Delta t)H}\| &\leq \frac{(\Delta t)^3}{12} \sum_{\gamma_1=1}^{\Gamma} \left\| \left[\sum_{\gamma_3=\gamma_1+1}^{\Gamma} H_{\gamma_3}, \left[\sum_{\gamma_2=\gamma_1+1}^{\Gamma} H_{\gamma_2}, H_{\gamma_1} \right] \right] \right\| \\ &\quad + \frac{(\Delta t)^3}{24} \sum_{\gamma_1=1}^{\Gamma} \left\| [H_{\gamma_1}, [H_{\gamma_1}, \sum_{\gamma_2=\gamma_1+1}^{\Gamma} H_{\gamma_2}]] \right\| \end{aligned} \quad (\text{A.4})$$

Our Hamiltonian is $H = H_1 + H_2 + H_3$, thus the error bound is

$$\begin{aligned} \|S_2(t) - e^{-itH}\| &\leq \frac{(\Delta t)^3}{12} \sum_{l=1}^3 \left\| \left[\sum_{n=l+1}^3 H_n, \left[\sum_{m=l+1}^3 H_m, H_l \right] \right] \right\| \\ &\quad + \frac{(\Delta t)^3}{24} \sum_{l=1}^3 \left\| [H_l, [H_l, \sum_{m=l+1}^3 H_m]] \right\| \\ &\leq \frac{(\Delta t)^3}{12} \sum_{l=1}^3 \sum_{n=l+1}^3 \sum_{m=l+1}^3 \|H_n[H_m, H_l] - [H_m, H_l]H_n\| \\ &\quad + \frac{(\Delta t)^3}{24} \sum_{l=1}^3 \sum_{m=l+1}^3 \|H_l[H_l, H_m] - [H_l, H_m]H_l\| \\ &\leq \frac{(\Delta t)^3}{6} \sum_{l=1}^3 \sum_{n=l+1}^3 \sum_{m=l+1}^3 \|H_n\| \|H_m, H_l\| \\ &\quad + \frac{(\Delta t)^3}{12} \sum_{l=1}^3 \sum_{m=l+1}^3 \|H_l\| \|H_l, H_m\| \\ &= \frac{(\Delta t)^3}{6} W_1 + \frac{(\Delta t)^3}{12} W_2 \end{aligned} \quad (\text{A.5})$$

where

$$\begin{aligned} W_1 &= \sum_{l=1}^3 \sum_{n=l+1}^3 \sum_{m=l+1}^3 \|H_n\| \|H_m, H_l\| \\ W_2 &= \sum_{l=1}^3 \sum_{m=l+1}^3 \|H_l\| \|H_l, H_m\| \end{aligned} \quad (\text{A.6})$$

According to (A.1), we have

$$\begin{aligned}
W_1 &= \sum_{n=2}^3 \sum_{m=2}^3 \|H_n\| \| [H_m, H_1] \| + \|H_3\| \| [H_3, H_2] \| \\
&= \|H_2\| (\| [H_2, H_1] \| + \| [H_3, H_1] \|) \\
&\quad + \|H_3\| (\| [H_2, H_1] \| + \| [H_3, H_1] \| + \| [H_3, H_2] \|) \\
&\sim 9(18g + 36g\lambda) + 18\lambda(18g + 36g\lambda + 18\lambda) \\
&= 162(g + 2g\lambda) + 324\lambda(g + 2g\lambda + \lambda) \\
&= 162g + 648g\lambda^2 + 648g\lambda + 324\lambda^2
\end{aligned} \tag{A.7}$$

and

$$\begin{aligned}
W_2 &= \sum_{m=2}^3 \|H_1\| \| [H_1, H_m] \| + \|H_2\| \| [H_2, H_3] \| \\
&= \|H_1\| (\| [H_1, H_2] \| + \| [H_1, H_3] \|) + \|H_2\| \| [H_2, H_3] \| \\
&\sim 18g(18g + 36g\lambda) + 9(18\lambda) \\
&= 324g^2 + 648g^2\lambda + 162\lambda
\end{aligned} \tag{A.8}$$

The evolution in Sec. 6 is from $(0, r)$ to (p, r) on $l : \lambda = r$ with g increasing from 0 to p in $N = p/\Delta g$ steps. Denote $g = n\Delta g$, then the total error is

$$\begin{aligned}
\epsilon &\leq \frac{(\Delta t)^3}{6} \sum_{n=1}^N W_{1,n} + \frac{(\Delta t)^3}{12} \sum_{m=1}^N \Delta_m W_{2,m} \\
&\sim \frac{(\Delta t)^3}{6} \sum_{n=1}^N (162g + 648g\lambda^2 + 648g\lambda + 324\lambda^2) \\
&\quad + \frac{(\Delta t)^3}{12} \sum_{m=1}^N (324g^2 + 648g^2\lambda + 162\lambda) \\
&= (\Delta t)^3 \sum_{n=1}^N (27g + 108g\lambda^2 + 108g\lambda + 54\lambda^2) \\
&\quad + (\Delta t)^3 \sum_{m=1}^N (27g^2 + 54g^2\lambda + 13.5\lambda) \\
&= (\Delta t)^3 \sum_{n=1}^N (27g + 108g\lambda^2 + 108g\lambda + 54\lambda^2 \\
&\quad + 27g^2 + 54g^2\lambda + 13.5\lambda) \\
&= (\Delta t)^3 \sum_{n=1}^N (27g + 108gr^2 + 108gr + 54r^2 \\
&\quad + 27g^2 + 54g^2r + 13.5r)
\end{aligned} \tag{A.9}$$

Besides, we have

$$\begin{aligned}\sum_{n=1}^N g &= \sum_{n=1}^N (n\Delta g) \approx \Delta g \frac{N^2}{2} = \frac{1}{2}pN \\ \sum_{n=1}^N g^2 &= \sum_{n=1}^N (n\Delta g)^2 \approx \Delta g^2 \frac{N^3}{3} = \frac{1}{3}p^2 N\end{aligned}\tag{A.10}$$

Rewrite (A.9) with (A.10), we have

$$\begin{aligned}\epsilon &\lesssim (\Delta t)^3 (27\frac{1}{2}pN + 108\frac{1}{2}pNr^2 + 108\frac{1}{2}pNr + 54r^2N \\ &\quad + 54\frac{1}{3}p^2N + 54\frac{1}{3}p^2Nr + 13.5rN) \\ &= (\Delta t)^3 N (13.5p + 54pr^2 + 54pr + 54r^2 \\ &\quad + 9p^2 + 18p^2r + 13.5r)\end{aligned}\tag{A.11}$$

Acknowledgments

This work was supported by National Science Foundation of China (Grant No. 12075059).

References

- [1] K. G. Wilson. Confinement of quarks. *Phys. Rev. D* **10** (1974) 2445.
- [2] E. A. Martinez et al. Real-time dynamics of lattice gauge theories with a few-qubit quantum computer. *Nature* **534** (2016) 516.
- [3] E. Zohar, D. González-Cuadra, and J. I. Cirac. Quantum simulation of the abelian-higgs lattice gauge theory with ultracold atoms. *New Journal of Physics* **19** (2017) 063038.
- [4] F. M. Surace et al. Lattice gauge theories and string dynamics in rydberg atom quantum simulators. *Phys. Rev. X* **10** (2020) 021041.
- [5] X. Cui, Y. Shi, and J. Yang. Circuit-based digital adiabatic quantum simulation and pseudoquantum simulation as new approaches to lattice gauge theory. *J. High Energ. Phys.* **160** (2020) .
- [6] X. Cui and Y. Shi. Trotter errors in digital adiabatic quantum simulation of quantum \mathbb{Z}_2 lattice gauge theory. *International Journal of Modern Physics B* **34** (2020) 2050292.
- [7] I. S. Tupitsyn, A. Kitaev, N. V. Prokof'ev, and P. C. E. Stamp. Topological multicritical point in the phase diagram of the toric code model and three-dimensional lattice gauge higgs model. *Phys. Rev. B* **82** (2010) 085114.
- [8] E. Fradkin and S. H. Shenker. Phase diagrams of lattice gauge theories with higgs fields. *Phys. Rev. D* **19** (1979) 3682.
- [9] J. L. Banks and D. K. Sinclair. Hamiltonian Calculations for the Z2 Lattice Gauge Theory With Matter Fields. *Phys. Rev. D* **23** (1981) 2962.
- [10] Z. Nussinov. A Derivation of the Fradkin-Shenker result from duality: Links to spin systems in external magnetic fields and percolation crossovers. *Phys. Rev. D* **72** (2005) 054509.
- [11] J. Vidal, S. Dusuel, and K. P. Schmidt. Low-energy effective theory of the toric code model in a parallel field. *Phys. Rev. B* **79** (2009) 033109.
- [12] G. A. Jongeward, J. D. Stack, and C. Jayaprakash. Monte Carlo calculations on \mathbb{Z}_2 gauge-Higgs theories. *Phys. Rev. D* **21** (1980) 3360.
- [13] M. Creutz. Phase diagrams for coupled spin-gauge systems. *Phys. Rev. D* **21** (1980) 1006.
- [14] A. M. Somoza, P. Serna, and A. Nahum. Self-dual criticality in three-dimensional \mathbb{Z}_2 gauge theory with matter. *arXiv:2012.15845*.
- [15] N. Hatano and M. Suzuki. Finding Exponential Product Formulas of Higher Orders. *Springer Berlin Heidelberg*, Berlin, Heidelberg (2005).
- [16] M. C. Tran, Y. Su, D. Carney, and J. M. Taylor. Faster digital quantum simulation by symmetry protection. *PRX Quantum* **2** (2021) 010323.
- [17] A. M. Childs, Y. Su, M. C. Tran, N. Wiebe, and S. C. Zhu. Theory of trotter error with commutator scaling. *Phys. Rev. X* **11** (2021).